JOURNAL OF GEOPHYSICAL RESEARCH, VOL. 101, NO. B11, PAGES 25,321–25,336, NOVEMBER 10, 1996

Complexity of seismicity due to highly rate-dependent friction

A. Cochard[1] and R. Madariaga

Département de Sismologie, Institut de Physique du Globe de Paris

Abstract. We study a simple antiplane fault of finite length embedded in a homogeneous, isotropic, elastic solid in order to understand the origin of seismic source heterogeneity in the presence of nonlinear rate-dependent friction. All the mechanical properties of the medium and friction are assumed to be homogeneous. Starting from a heterogeneous initial stress distribution, we apply a slowly increasing uniform stress load far from the fault and we simulate the seismicity for more than 20,000 events, in some cases. The style of seismicity produced by this model is determined by a control parameter which measures the degree of rate dependence of friction. For classical friction models with rate-independent friction, no complexity appears and seismicity is perfectly periodic. For weakly rate-dependent friction, seismicity becomes slightly nonperiodic but most events are still characteristic earthquakes. When friction is highly rate-dependent, seismicity is completely irregular and ruptures of all sizes occur inside the fault. Highly rate-dependent friction destabilizes the healing process, producing premature healing of slip and partial stress drop. Premature healing causes rupture to take the form of narrow, propagating slip episodes, the so-called *Heaton*'s [1990] pulses. Partial stress drop produces large variations in the state of stress which, in turn, produce earthquakes of different sizes. We make the conjecture that all models in which static stress drop is only a fraction of the dynamic stress drop produce stress heterogeneity.

Introduction

A fundamental problem for the understanding of seismicity and the nature of large earthquakes is the origin of stress and slip complexity on seismic faults. Careful studies of seismicity have evidenced the complexity of its space-time distribution. Similarly, numerous detailed studies of slip distribution during individual earthquakes show extremely large variations of slip on the fault. A common feature of these studies is the clear presence of irregularities and complexity of seismic sources. Although the evidence for complexity is overwhelming, the dynamics of faulting is still poorly understood. Many authors seem to favor a model where complexity is attributed to fault segmentation or to variations of material properties of the fault plane. The most common model used to explain complexity is the ubiquitous presence of heterogeneities called barriers or asperities. Barriers are places of high strength that can stop ruptures [*Das and Aki*, 1977]. Asperities, on the other hand, are places of high stress release or, equivalently, of relatively large slip [*Kanamori and Stewart*, 1978]. Asperities are sometimes also considered as places of high strength that fail with a relatively large stress release because stress has been accumulated on these places that did not fail during previous earthquakes which occurred in their vicinity. Indeed, *Das and Kostrov* [1988] define barriers and asperities by the same constitutive law.

A common feature of these models is that barriers and asperities are considered to be due to fixed geometrical or material properties of the fault. However, asperities viewed as regions of high stress release may be dynamically created. This was demonstrated by *Carlson and Langer* [1989] for the very simple *Burridge and Knopoff* [1967] model (hereinafter referred to as the Burridge-Knopoff model) using a particular rate-weakening friction law. They showed that in an otherwise perfectly homogeneous model, stress may become spontaneously heterogeneous due to nonlinear instabilities in the velocity-weakening friction law they used. *Rice* [1993] argued that this model was, in fact, "intrinsically discrete" because it lacked an intrinsic length scale in the friction law. Using a quasi-static approximation of the wave equation, he showed that if the grid size was smaller than a characteristic length scale (the nucleation size) related to the friction law he used, small-event complexity disappeared. Only when "oversized" cells were used, roughly simulating independent fault segment, did he observed small-event complexity [see also *Ben-Zion and Rice*, 1993]. Recently, *Rice*

[1]Now at Division of Applied Sciences, Harvard University, Cambridge, Massachusetts.

Paper number 96JB02095.
0148-0227/96/96JB-02095$09.00

and Ben-Zion [1996] have extended *Rice*'s [1993] quasi-static study to the fully elastodynamic case; the results remain unchanged: no small-event complexity develops. On the other hand, more recent studies of the Burridge-Knopoff model [*Shaw*, 1995] or a more sophisticated version of it that incorporates long-range interactions [*Langer et al.*, 1996] have shown that heterogeneity persists even when a friction law that has a characteristic length is used. In order to reduce computer time, earthquakes in these studies were triggered by a more or less instantaneous stress drop, during which no characteristic length acts, allowing again for small-event complexity. Indeed, often in these studies, no events with length between the nucleation size and the analog of the seismogenic depth are observed and changing the triggering mechanism results in a change of the properties of the small events (i.e., less than the seismogenic depth).

We use a simple antiplane fracture model with a friction law that can be highly rate-dependent but that is regularized by a slip-weakening zone which introduces a finite nucleation zone [*Madariaga and Cochard*, 1996]. We also use an artificial stress drop in order to trigger the events and generally also observe a small-event complexity associated with this triggering. When friction is not or is mildly rate-dependent, we observe a periodic sequence of crack events; but, when friction is highly rate-dependent, we observe, in addition to the artificial small-event complexity, a broad range of short-time rupture duration events (pulses) of length between the nucleation zone and the system size.

We think that the opposition between intrinsic versus dynamically sustained strength heterogeneity comes from a problem of interpretation of what rupture resistance on an active fault really is. Like in fracture mechanics, rupture resistance is not a simple point function like stress but is the product of the square of peak frictional stress times a certain length scale. Thus fault segments that have very narrow stress concentrations are likely to be very strong, while areas that have longer (fatter) stress concentrations are much weaker and prone to generate small and large events. In models with intrinsic heterogeneity, rupture resistance is fixed (quenched) on the fault. In our model, rupture resistance changes dynamically because the length scale of the stress concentrations evolves with time. The only difference between intrinsically heterogeneous models and ours is that in our case, rupture resistance changes slowly with time due to elastodynamic interaction and partial stress drop. It is clear that material heterogeneity is likely to play an important part in the Earth, especially to explain repetitive earthquakes such as those studied by *Vidale et al.* [1994] or earthquakes at Parkfield. Also, material heterogeneity may also be responsible for pulses, as shown by *Das and Kostrov* [1988]. We wanted to study effects of nonlinear dynamics only and so used a homogeneous fault. If we had introduced some quenched heterogeneity in rupture resistance, this would have simply increased the instability of the locking mechanism and thus enhanced heterogeneity.

Definition of the Model: Antiplane Fault

We study the elastodynamic field due to a flat antiplane crack Γ that extends along the $z = 0$ line in a homogeneous, linearly elastic medium of rigidity μ, density ρ, and shear wave velocity $\beta = \sqrt{\mu/\rho}$ (Figure 1).

The only displacement component in this case is $u_y(x, z, t)$ that will be denoted simply u in the following, and the only nonzero elements of the stress tensor are σ_{yx} and σ_{yz}. Antiplane displacement satisfies a scalar wave equation $\beta^{-2}\ddot{u} = \nabla^2 u$, where the dots indicate the time derivative. Boundary conditions on the plane of the fault $z = 0$ are $\sigma_{yz}(x,t) = \Delta T(x,t)$ on Γ, $D(x,t) = 0$ out of Γ, where the slip across the fault is defined as $D(x,t) = u(x,0^+,t) - u(x,0^-,t)$. The traction change $\Delta T(x,t)$ is related to the friction law that applies between the two walls of the crack. We are interested in studying the effect of a friction such that the absolute traction T_{abs} is a nonlinear function of slip $D(x,t)$ and of the slip velocity discontinuity $V(x,t) = \dot{D}(x,t)$. This boundary value problem can be solved only by numerical methods. As discussed by *Virieux and Madariaga* [1982] and also noticed by *Andrews* [1976, 1985], finite differences are too inaccurate because of high-frequency dispersion, so that we adopted the new boundary integral equation (BIE) method proposed by *Cochard and Madariaga* [1994].

The BIE relating traction (stress) change ΔT to slip velocity on the fault is

$$\Delta T(x,t) = -\frac{\mu}{2\beta}V(x,t) - \frac{\mu}{2\pi}\int\int_{\Gamma}\int_{0}^{\tau_m}\frac{\sqrt{(t-\tau)^2-(x-\xi)^2/\beta^2}}{(t-\tau)(x-\xi)}\frac{\partial}{\partial\xi}V(\xi,\tau)d\tau d\xi \quad (1)$$

with $\tau_m = \max(0, t - \|x-\xi\|/\beta)$. This integral equation has a removable singularity at $\xi \to x$, where it has to be interpreted in the usual sense of Cauchy integrals. The first term of the right-hand side is the instantaneous traction change produced by a corresponding change in slip velocity. The second term is the effect of long-range interactions between the dislocation distribution at different places on the fault. The negative signs mean that

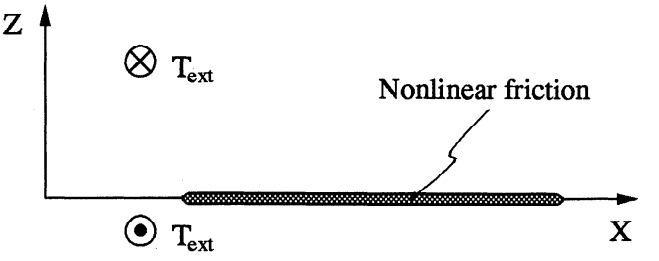

Figure 1. Geometry of the antiplane shear crack. The fault area is located on the $z = 0$ plane of an infinite, homogeneous, isotropic medium. The system is invariant with respect to translation along the y axis. No opening of the crack is allowed. Slip u and discontinuity of slip are allowed only along the y direction. The fault can expand along the x axis.

positive slip produces negative stress increase (positive stress drop).

As noted above, the BIE (1) relates slip rate to traction changes on the fault. The absolute traction on the fault is the sum of the stress change and the externally imposed stress load or driving stress $T_{\text{ext}}(x,t)$:

$$T_{\text{abs}}(x,t) = \Delta T(x,t) + T_{\text{ext}}(x,t) \ . \tag{2}$$

At $t = 0$, before slip occurs, the absolute traction $T_{\text{abs}}(x,0) = T_{\text{ext}}(x,0)$, which is the initial stress. After an earthquake occurs and all elastic wave activity comes to an end, we reset the system and redefine the initial stress from the final stress of the previous event. External stress is assumed to increase at a low tectonic rate ϵ defined by

$$T_{\text{ext}}(x,t) = \epsilon t \ . \tag{3}$$

Numerical Simulation of Earthquakes

Discretization of the Integral Equation

We divide the fault line $z = 0$ into segments of equal length Δx, and we discretize time by taking equal intervals Δt. We introduce the following simple discretization of the slip velocity field

$$V(x,t) = \sum_{j,m} V_{j,m} d(x,t;x_j,t_m) \tag{4}$$

where $d(x,t;x_j,t_m)$ is the boxcar function:

$$\begin{aligned} d(x,t;x_j,t_m) &= 1 \quad \begin{cases} x_j \le x < x_{j+1} \\ t_m \le t < t_{m+1} \end{cases} \\ d(x,t;x_j,t_m) &= 0 \quad \text{otherwise.} \end{aligned} \tag{5}$$

This makes the slip velocity field, and any other variable such as traction, constant on each space-time grid element. *Cochard and Madariaga* [1994] reduced the BIE (1) to a discrete problem by collocation at the knots $x_i + \Delta x/2$ and times $t_n + \epsilon_t \Delta t$, with $\epsilon_t \in [0,1]$. Writing

$$\Delta T_{i,n} = \Delta T(x_i + \Delta x/2, t_n + \epsilon_t \Delta t) \tag{6}$$

we get the linear system

$$\Delta T_{i,n} = -\frac{\mu}{2\beta} V_{i,n} - \frac{\mu}{2\beta} \sum_{\substack{j \\ m \le n-1}} K_{i-j,n-m} V_{j,m} \tag{7}$$

where the analytic formula for the kernel $K_{i,n}$ is computed replacing the velocity distribution expression (4) into the BIE (1). Explicit expressions are given by *Cochard and Madariaga* [1994] (in which the first term of equation (15) should be removed; it affects only $K_{0,0}$ which does not appear in the summation (7)). By trial and error we adopted $\epsilon_t = 1$, which gives the best and most stable numerical results. Then using the relation between absolute and relative stress (2), we obtain the following discrete BIE (DBIE)

$$T_{\text{abs}_{i,n}} = -\frac{\mu}{2\beta} V_{i,n} + T_{\text{ext}_{i,n}} - \frac{\mu}{2\beta} \sum_{m=0}^{n-1} \sum_{j} V_{j,m} K_{i-j,n-m} \tag{8}$$

where $T_{\text{abs}_{i,n}}$ is the highly nonlinear friction across the fault plane (for moving points).

Numerical Solution of the Boundary Integral Equation

At time step n we distinguish slipping boundary elements for which we want to calculate the slip rate $V_{i,n}$ from boundary elements that are locked, for which we only want to calculate the absolute traction $T_{\text{abs}_{i,n}}$. At step n we make an initial estimate of $T_{\text{abs}_{i,n}}$ using the DBIE (8) assuming that $V_{i,n} = 0$. If the velocity of a given point was zero at the previous time step ($V_{i,n-1} = 0$) and if $T_{\text{abs}_{i,n}}$ is less than the rupture threshold T_{thres_i} at this point, then the point remains locked and $T_{\text{abs}_{i,n}}$ becomes the value of the absolute traction for the current time step. On the other hand, if the velocity of a given point was not zero in the previous time step ($V_{i,n-1} \neq 0$) or if $T_{\text{abs}_{i,n}}$ becomes greater than the threshold, the point begins to move and the absolute traction is then given by the friction law that applies at this point and one has to solve the DBIE (8) simultaneously for the velocity and for the friction, as described in the next section.

Most of the computer time in each time step is consumed by the evaluation of the discrete space-time convolution in (8). The space convolution is computed by fast Fourier transform (FFT) methods, while the time convolution is computed directly by explicit summation. We get

$$\begin{aligned} S_{i,n} &= \sum_{m=0}^{n-1} \sum_{j} K_{i-j,n-m} V_{j,m} \\ &= \sum_{m=0}^{n-1} K_{i,n-m} \star V_{i,m} \end{aligned} \tag{9}$$

where star states for space convolution. Defining the Fourier transform by $\mathcal{F}$ and using the convolution theorem, we find

$$S_{i,n} = \mathcal{F}^{-1} \left\{ \sum_{m} \mathcal{F}[K_{i,n-m}] \times \mathcal{F}[V_{i,m}] \right\} \ . \tag{10}$$

A similar scheme has been used by *Andrews* [1985], and this is also formally equivalent to the procedure devised by *Perrin et al.* [1995], in which a spectral instead of a cellular method is used. The results of the direct FFTs can be saved at each time step and used for subsequent time intervals.

At time step n the evaluation of $S_{i,n}$ involves one FFT on a one-dimensional (1-D) array of length $2I$ (where $I\Delta x$ is the total size of the fault and the factor of 2 takes into account the necessary zero padding), one multiplication, one summation along the time dimension on a 2-D array of size $n \times 2I$, and one inverse FFT on an array of the same size as for the direct FFT. Thus, for

the evolution of a fault of I elements up to time step N, the number of operations required for the computation of $S_{i,n}$ is

$$2\,IN\left[\alpha\log_2(I)+\frac{N-1}{2}\right] \tag{11}$$

where α is the proportionality constant or order 1 involved in the FFT algorithm. Therefore the number of operations is $\mathcal{O}(IN^2)$. The computation of the time convolution by FFT would not be efficient because we need the result of the convolution at only one time step (the current step n). However, time domain FFTs are useful once all points of the fault have healed because we can then evaluate the stress field up to any desired time in a single step.

Slip- and State-Dependent Friction Law

Extensive work on rock friction has been discussed recently by *Dieterich* [1992]. Experimental evidence shows that friction laws at low slip rates should at least include three elements: (1) Direct stress change for abrupt changes in slip velocity followed by (2) an evolving phase characterized by an intrinsic time constant leading through exponential decay to (3) a velocity weakening or strengthening at steady state (ss) slip. When the friction is velocity weakening (a necessary condition for instability), steady state frictional stress is related to the logarithm of steady state slip rate by $T_{ss}(V_{ss}) = A_1 - A_2\log(V_{ss})$, $A_{1,2}$ constants greater than zero. This type of friction laws (including those of *Ruina* [1983]) will be hereinafter referred to as Dieterich-Ruina laws. Previous simulations using rate and state friction laws [*Okubo*, 1989] have shown that slip-weakening and rate- and state-dependent frictions produce similar behavior near the rupture front. As the contribution of the direct effect is likely to be strongest precisely near the rupture front (i.e., for fast rate changes), we have decided, after considering several alternatives, for the sake of simplicity, to approximately mimic the direct effect by using a slip-weakening model instead. Indeed, other simulations [*Shibazaki and Matsu'ura*, 1992] using slip-weakening friction laws are in qualitative agreement with experiments of stick-slip shear failure as regards to the beginning of slip. The characteristic distance introduced by this way in the friction law makes it impossible for events less than a certain small length to become unstable and grow into fully fledged earthquakes. This minimum earthquake size is also a well-known feature of rate- and state-dependent frictions [e.g., *Dieterich*, 1992; *Rice*, 1993]. Finally, for reasons explained later, we chose a linear decrease of friction with steady state velocity instead of a logarithmic one. The laboratory-based friction laws were obtained for low values of slip rate (less than the seismic slip rate by 2 orders of magnitude), so that they are strictly valid only during the nucleation process. It is not unlikely that friction laws during earthquakes be very different from those obtained in the laboratory because of other phenomena that can become predominant, e.g., frictional heating, opening modes, etc. In fact, using a Dieterich-Ruina type friction law at seismogenic confining pressures would lead to extensive melting during the rupture process, which is seldom observed on exhumed faults. Actually, any physical process that introduces variations in normal stress during slip may cause a velocity weakening behavior such as the "acoustic fluidization" of *Melosh* [1979, 1996], due to the propagation of acoustic waves along the interface, or such as faulting with different elastic properties on each side of the fault [*Andrews and Ben-Zion*, 1996].

In order to avoid the numerical problems that appear during the transition from steady slip to unstable, fully dynamic faulting, we introduced a small artificial instantaneous stress drop $\Delta\sigma$ in order to initiate fault slip. If this parameter were not present, the initiation would be induced only by the tectonic loading: simulating this accelerating slip phase is beyond the scope of the present paper. The same kind of small artificial stress drop has been used by *Carlson et al.* [1991] in their Burridge-Knopoff model and by *Langer et al.* [1996] for a 2-D antiplane fault that obeys the Klein-Gordon equation instead of the wave equation. This arbitrary stress drop makes the system intrinsically discrete in the terminology of *Rice* [1993] because events that affect only one grid element are possible, whereas the minimum size of events should not be less than the nucleation size. The effects of nonzero $\Delta\sigma$ will be discussed in the appendix.

Besides this instantaneous stress drop, friction as a function of slip D and state θ, at a given point of the fault, is given by the intersection of the following three plane segments:

$$\begin{aligned} T_{\text{abs}}(D,\theta) &= (T_{\text{thres}}-\Delta\sigma)\left(1-\frac{D}{U_0}\right) && \begin{cases} D\le U_0 \\ \theta\ge\theta_1 \end{cases} \\ &= 0 && \begin{cases} D\ge U_0 \\ \theta\ge\theta_0 \end{cases} \\ &= T_{\text{sp}}\left(1-\frac{\theta}{\theta_0}\right) && \begin{cases} \theta\le\theta_0 \\ \theta\le\theta_1 \end{cases} \end{aligned} \tag{12}$$

with

$$\begin{aligned} \theta_1 &= \theta_0\frac{D-U_1}{U_0-U_1} \\ U_1 &= -U_0\frac{T_{\text{sp}}-T_{\text{thres}}+\Delta\sigma}{T_{\text{thres}}-\Delta\sigma}. \end{aligned}$$

This apparently complex definition becomes much clearer when one looks, instead, at its graphical representation in Figure 2. The slip D is measured from the beginning of the current slip episode, and the state (memory) variable θ follows the evolution law

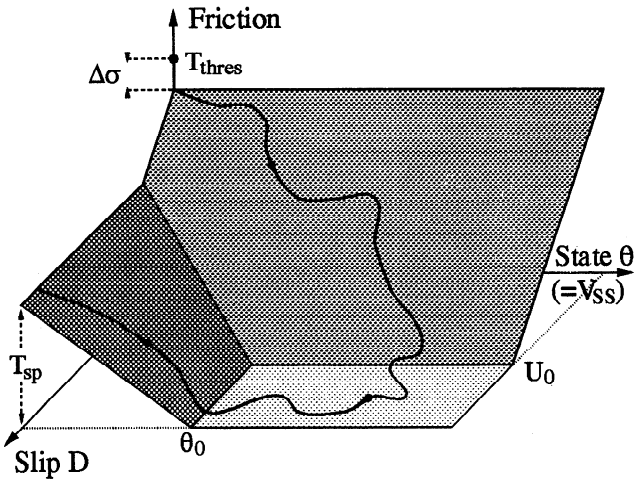

Figure 2. The constitutive law studied in this paper. The solid line shows a typical point trajectory. The friction is slip weakening (with characteristic distance U_0) at the beginning of the movement and state-dependent at the end. State dependence is related throughout equation (13) to rate dependence, which will be varied in the simulations by varying the parameter T_{sp}, keeping the others parameters θ_0 and U_0 fixed. At the very beginning of the movement, slip is triggered by a small stress drop characterized by $\Delta\sigma$.

$$\frac{d\theta}{dt} = -\frac{\beta}{D_c}(\theta - V) \tag{13}$$

where D_c is a characteristic distance. At steady state ($\dot{\theta} = 0$), θ_{ss} is equal to the slip rate V; thus θ differs from V only during rapid changes of slip rate. If $T_{sp} = 0$, friction is pure slip-weakening friction with slip-weakening distance U_0. During the process of rupture a particular point of the fault schematically follows the curve in Figure 2. At the beginning of the movement the point is located on the slip-weakening plane. As slip rate and θ increase, friction reduces to zero and becomes independent of D and θ as in the classical friction laws with constant static and kinematic friction. Finally, at the end of the movement, as slip rate decreases, the point climbs up the rate-dependent plane. For moderately big events the point trajectory can switch directly from the slip-weakening plane to the rate-dependent plane. The most important feature of the friction law is that it produces partial stress drop whenever T_{sp} is larger than 0. The reason is that residual stress on the fault increases as slip rate decreases. As we will show, this produces early healing of the fault, reduced slip, and therefore partial stress drop [*Brune*, 1970; *Heaton*, 1990].

The friction law, (12) and (13), possesses two characteristic lengths U_0 and D_c that are required to avoid numerical artifacts caused by fast changes in slip velocity at the beginning and at the healing of slip. In massive wave equations (like the Klein-Gordon equation of *Langer et al.* [1996]) these rapid changes are limited by the presence of the pseudomass term. Of course, this regularization at small length scale is also provided by the classical rate and state friction laws. The advantage of the present formulation is that we can study the healing phases independently from the beginning of slip, varying the parameters T_{sp} and θ_0. This was done also (for a single seismic event) by *Beeler and Tullis* [1996], who had a pure slip-weakening friction law at the beginning of the movement, and once the displacement became greater than the slip-weakening distance, the friction became rate- and state-dependent. The particular choice of friction law (12) has the advantage that the nonlinear integral equation (8) has an analytical solution at every time step, so that it does not require an iterative procedure as would be necessary if we used the Dieterich-Ruina logarithmic friction laws. More importantly, the linear velocity dependence allows a high velocity dependence over a wide velocity range.

Modeling Long-Term Seismicity in a Uniform Antiplane Fault

In order to study the seismicity on the fault, we start the simulation from an initial random stress T_{ext} on a locked fault ($V_{i,n} = 0$ for all i). The initial stress can be either a random distribution smoothed in order that a big event occurs soon (as for the simulations presented in this paper) or the stress field obtained at the end of a previous simulation. The advantage of using a stress distribution taken from a previous run is that steady state seismicity is quickly reached. Tectonic loading is simulated by increasing T_{ext} uniformly across the fault and linearly with time as shown by (3). When frictional resistance T_{thres} is eventually overcome somewhere on the fault, an event occurs. The event is triggered by the small stress drop $\Delta\sigma$, and it either stops quickly before reaching the critical size or it reaches this critical size and it becomes a "seismic" event in our fault. Once all the points of the fault have locked, the stress field keeps changing for a while until all the available energy is evacuated by the seismic waves. When the stress variation is less than a prescribed accuracy, the event is considered to be finished. Then T_{ext} can be increased instantaneously (in the program) by a uniform amount such that the point of the fault of maximum stress reaches the threshold T_{thres}. Then the next dynamic event begins.

The variables in the numerical simulations were rendered nondimensional by the following choices: stresses were scaled with respect to the threshold T_{thres}, and we scaled fault length by the unit step Δx used to discretize the fault. Scaling of all the other variables in the BIE is determined by these two choices. For instance, slip velocity scales like $(2T_{thres}/\mu)\beta$, slip by $(2T_{thres}/\mu)\Delta x$, and time by $\Delta x/\beta$. The factor of 2 is introduced to eliminate the 1/2 factor in the dimensionless version of the DBIE (8). There are two main timescales in our problem. The fast one, related to fast "seismic" ruptures, is scaled by $\Delta x/\beta$. The slow timescale is due to the slowly increasing tectonic load defined by ϵ in

(3). We observe from this equation that T_{ext} can be used as a measure of the time involved in the seismic cycle. Assuming complete stress drop during an event, an estimate of the recurrence interval between event is $t_{cyc} = T_{thres}/\epsilon$. The duration of an event, on the other hand, is $t_{evt} \simeq L/\beta$, where $L = I\,\Delta x$ is the total length of the fault. Thus we estimate the dimensionless loading rate parameter $\hat{\epsilon}$ by $\hat{\epsilon} \simeq (t_{evt}/t_{cyc})/I$ (here and in the following we use the circumflex notation to designate dimensionless variables). A value of 10^{-7} is a realistic value of t_{evt}/t_{cyc}. Here $\hat{\epsilon}$ has been fixed to 2×10^{-10} for all the simulations presented in this paper. In order to relate the two timescales, one simply has to multiply (or divide) by the value of $\hat{\epsilon}$.

In order to study the statistical properties of the observed seismicity, we have to introduce some additional parameters. Here ℓ is the length of a broken patch during an event. It is often different from the overall size of the event because for many events the rupture zone is discontinuous along the fault. Next, we define the moment M of an event as

$$M \propto \bar{D}\ell \tag{14}$$

with

$$\bar{D} = \frac{1}{\ell}\int \left[D^{final}(x) - D^{initial}(x)\right]\,dx\,. \tag{15}$$

$\bar{D}$ is the average slip, and we do not consider the constant μ factor in the definition of M. In the plots the normalized values of ℓ and M will be further divided by the number I of elements of the fault in order to compare simulations with different I. Let us finally define the average stress drop for one event as

$$\Delta T_{av} = \frac{1}{\ell}\int \left[T_{abs}^{initial}(x) - T_{abs}^{final}(x)\right]\,dx \tag{16}$$

where the summation extends over the broken patch. The parameters that appear in the friction law were adopted as follows, unless otherwise stated: $\Delta\sigma = 5 \times 10^{-2} T_{thres}$, $U_0 = (20\,T_{thres}/\mu)\Delta x$, and $D_c = 3\,\Delta x$; this corresponds to $\Delta\hat{\sigma} = 5 \times 10^{-2}$, $\hat{U}_0 = 10$, and $\hat{D}_c = 3$. (Let us remark on the different units of U_0 and D_c; the former is measured in units of fault slip, while D_c is measured in units of fault length.) Here $\theta_0 = (2\,T_{thres}/\mu)\beta$ (that is $\hat{\theta}_0 = 1$) is measured in units of slip velocity. It corresponds to a typical value of the slip rate, given by the radiation damping term (the instantaneous one) in the BIE (1) assuming complete stress drop. T_{sp}, measured in units of peak stress T_{thres}, will be varied between 0 and its highest acceptable value $T_{thres} - \Delta\sigma$, which means that $\hat{T}_{sp}$ will be varied between 0 and $1 - \Delta\hat{\sigma}$.

In our simulations we have to chose a dimensionless time step ($h = \beta\Delta t/\Delta x$) and used a value of 0.5 [see *Cochard and Madariaga*, 1994]. We used a CM-5 supercomputer. To give an idea, the simulation of an event on a fault of $I = 1025$ elements up to $N = 2048$ time steps requires about 45 s using 32 nodes.

Seismicity on a Fault With Increasing Rate Dependence of Friction

As noted by *Madariaga and Cochard* [1996] from a limited number of numerical simulations, the parameter that controls the spontaneous development of heterogeneity on the fault in our friction law is $\hat{T}_{sp}$. The θ_0 does intervene also but we have not performed a detailed study of its role so far. Let us just mention that its value has to be of order 1 (in dimensionless units) in order for the complexity to appear; this is intuitive since its contribution to the rate dependence is symmetric to that of T_{sp}: for θ_0 approaching zero, the friction law becomes effectively rate-independent, whatever the value of T_{sp}. In our numerical experiments we observe that the main characteristics of seismicity change radically as T_{sp} increases from 0 (i.e., classical slip-weakening friction) to T_{thres}. Seismic complexity increases as the control parameter increases. The increasing complexity

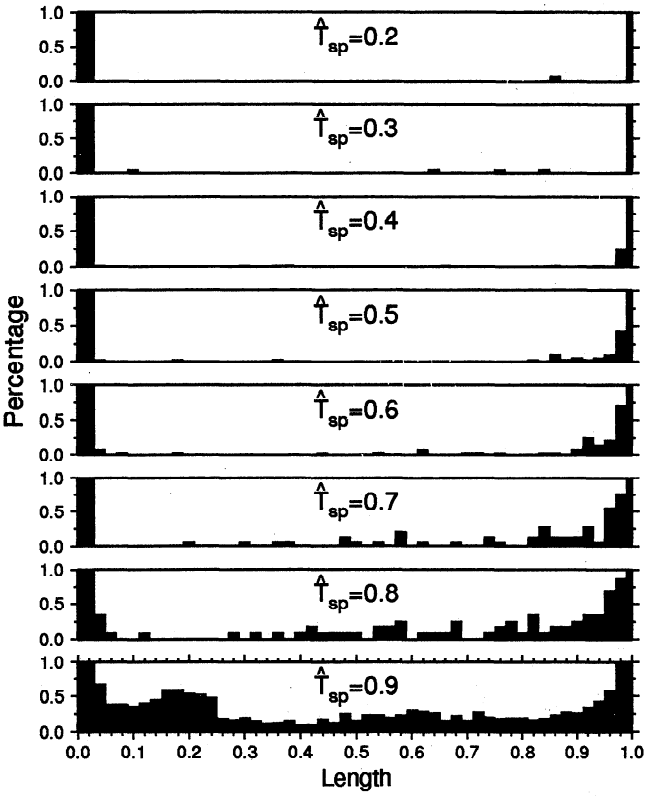

Figure 3. Histograms of lengths of each earthquake (normalized by the total length of the fault) for various values of the control parameter $\hat{T}_{sp}$. Each plot corresponds to the seismicity on a single, homogeneous fault, starting from a heterogeneous stress field and continuously increasing the loading stress. The circumflex indicates a dimensionless variable. The ordinate axis is truncated at 1% to allow for legibility owing to the high proportion of small and large events. (For $\hat{T}_{sp} = 0$ and 0.1 all the events break the whole fault.)

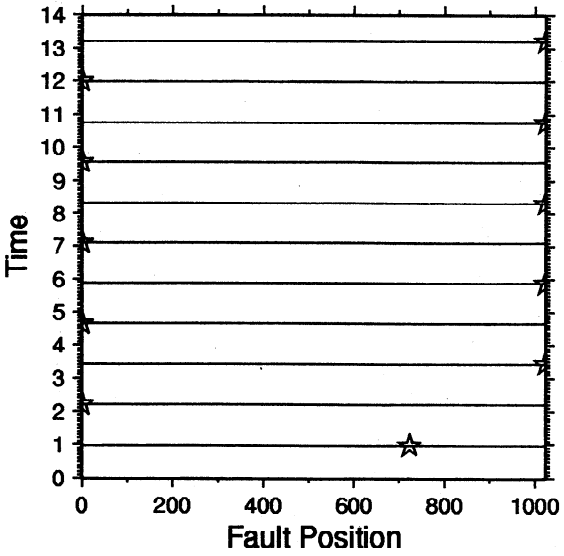

Figure 4. Seismicity on the fault as a function of time without any rate dependence of the constitutive law ($\hat{T}_{sp} = 0$). Each dot (and on similar figures to come) indicates that the cell at the corresponding fault position broke; hence a continuous horizontal segment represents an earthquake, the length of which is given by the length of the line. We thus see that in this case, seismicity is periodic and that all earthquakes break the whole fault. Stars indicate the locus of the epicenters, which are, after an initial transient stage, located alternatively on each end of the fault.

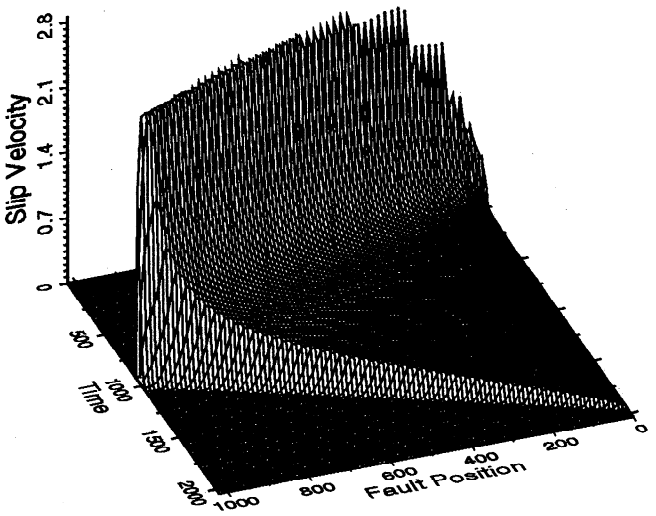

Figure 5. Slip velocity field for a typical event of the sequence for $\hat{T}_{sp} = 0$. It is typical of a crack-like event: each point on the fault plane stops moving when it receives the stopping phase owing to the abrupt arrest of the rupture front at the barrier.

can be clearly appreciated in Figure 3, which shows the histograms of the distribution of the sizes of the broken patches $\hat{\ell}$ as a function of $\hat{T}_{sp}$ ranging from 0.2 to 0.9 by step increments of 0.1. For each value of $\hat{T}_{sp}$ all the earthquakes for one seismic cycle are included. Only values between 0 and 1% are shown to allow for legibility because of the large proportion of very large and very small events. The histograms for $\hat{T}_{sp} = 0$ and 0.1 are not shown because in those cases all the events break the whole fault. We can see that as $\hat{T}_{sp}$ increases, events of increasingly different lengths $\hat{\ell}$ occur until finally, events of all sizes occur for $\hat{T}_{sp} = 0.9$. Let us describe in more detail the evolution of the seismicity as $\hat{T}_{sp}$ increases.

When $\hat{T}_{sp} = 0$, after a transient state whose duration depend on the initial stress, seismicity becomes perfectly periodic as shown in Figure 4. Each dot on this plot indicates that the corresponding point of the fault has slipped during one event. We thus see that for $\hat{T}_{sp} = 0$ the whole fault breaks during each earthquake. The stars in Figure 4 show the locus of the epicenters. Except for the first events of the sequence, all the other events are identical "characteristic" earthquakes. Velocity and stress field of one of these events are shown in Figures 5 and 6, respectively. The event starts at one end of the fault. The rupture propagates to the other end, where a stopping phase is emitted that propagates backward inside the fault and induces the arrest of the movement of all the points of the fault. This rupture is thus typical of a crack-like event. After all points have locked, the stress field decreases because of slip overshoot [*Madariaga*, 1976]. The points closest to the edges of the fault are the most strongly tied (the fault is stiffer near the edges), so that stress decreases less than for points situated near the middle of the fault. This explains why all the events begin near one end of the fault. Depending on details of the initial stress, the epicenters can be alternatively located on the two edges of the fault (as for the case shown) or always on the same side.

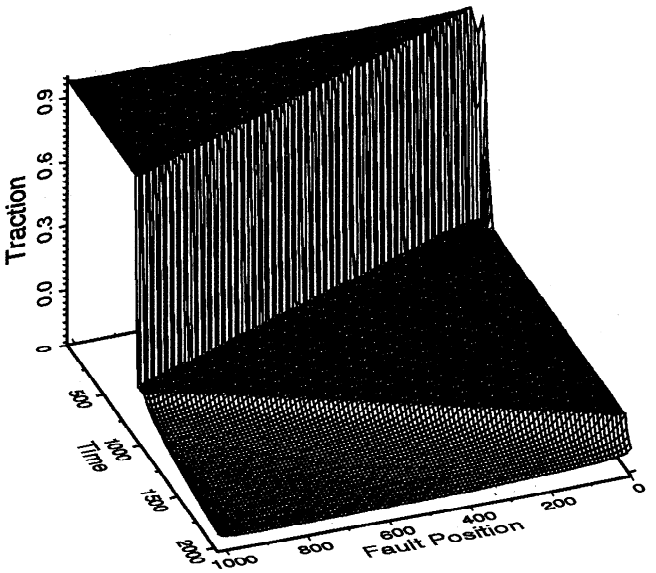

Figure 6. Stress field for the same event as in Figure 5 ($\hat{T}_{sp} = 0$). The stress is very homogeneous on the fault plane at the end of the event (after time 2000 the stress field is still evolving significantly but the plot is truncated for clarity).

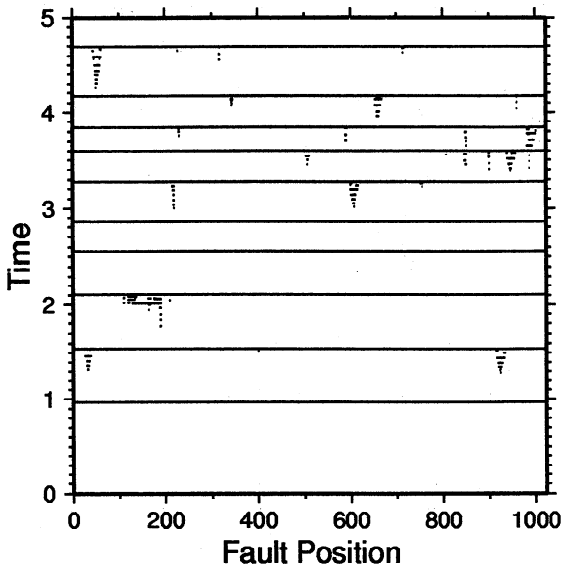

Figure 7. Seismicity on the fault as a function of time for a mild rate dependence of the constitutive law ($\hat{T}_{sp} = 0.3$). We now see a large number of small and localized events preceding a large one. These events are artifacts of the artificial initial stress drop $\Delta\sigma$ (see text for details). The other "real" earthquakes still break the whole fault but are now irregularly spaced in time.

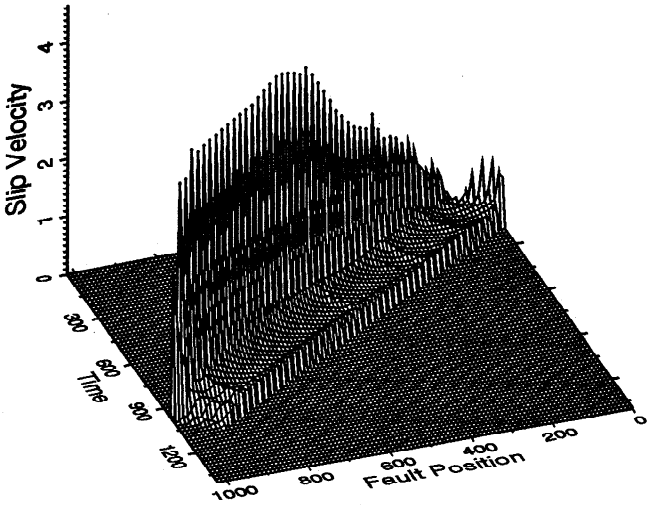

Figure 8. Slip velocity field for one event of the simulation for $\hat{T}_{sp} = 0.3$. It is typical of a crack-like event (with two stopping phases) but is much more irregular than for $\hat{T}_{sp} = 0$.

These results are not completely in agreement with those of *Nielsen et al.* [1995], who used a friction law resembling slip-weakening friction, in which the ratio of the relaxation distance to the total length of the fault is small enough (and yet much bigger than the corresponding value of the present study). They observe an aperiodic sequence of events. We wonder if this can be due to the use of the finite difference method, whose defects have been noted above. Nevertheless, they observe the following two distinct categories of events: small ones and big events that rupture the entire fault.

For $\hat{T}_{sp} = 0.1$ the characteristics of seismicity are qualitatively the same as in Figure 4. Because stress drop is no longer complete, the final stress after each event is higher and therefore closer to the threshold than for $\hat{T}_{sp} = 0$, resulting in earthquakes closer in time.

When $\hat{T}_{sp} = 0.2$ or 0.3, the seismicity (shown in Figure 7 for $\hat{T}_{sp} = 0.3$) is qualitatively different. It is now irregular in time, and the epicenters are located everywhere on the fault plane. We also see in Figure 3 a group of events with length less than 0.03 and a small moment. We discuss in the appendix the significance of these small events. Most of the other events break the whole fault, and in fact, those who do not break the whole fault have been stopped anyway by the barrier at one end of the fault. Let us note, however, that the stress field is now heterogeneous enough to stop these ruptures at the other end. The velocity and stress fields for a typical big event of the cycle for $\hat{T}_{sp} = 0.3$ are shown in Figures 8 and 9, respectively. This is still a crack-like event, as all of these big events are. As a consequence of having the epicenters in the middle of the fault, there are now two stopping phases (instead of only one for $\hat{T}_{sp} = 0$). The difference with the previous case is more important for the stress field. $\hat{T}_{sp}$ is now high enough to allow for the stress field to be higher somewhere inside the fault than on the edges (the reason is still the same; that is, the regions near the edges are more coupled to the fixed edges, but now this acts in the opposite way). This explains that the epicenters are no longer located near the edges of the fault.

When $\hat{T}_{sp} = 0.4$, the situation is qualitatively the same as for 0.3 except that some events do not reach

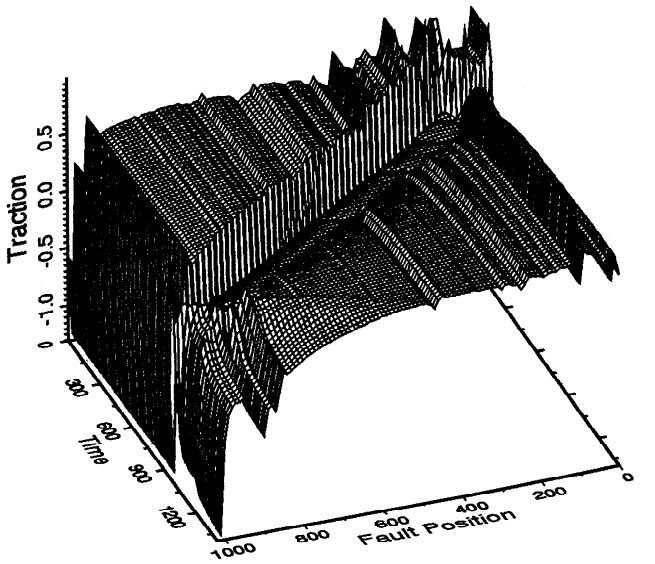

Figure 9. Stress field for the same event as in Figure 8 ($\hat{T}_{sp} = 0.3$). The stress is more heterogeneous on the fault plane than for $\hat{T}_{sp} = 0$, but it is not enough to allow for stopping events before the barriers.

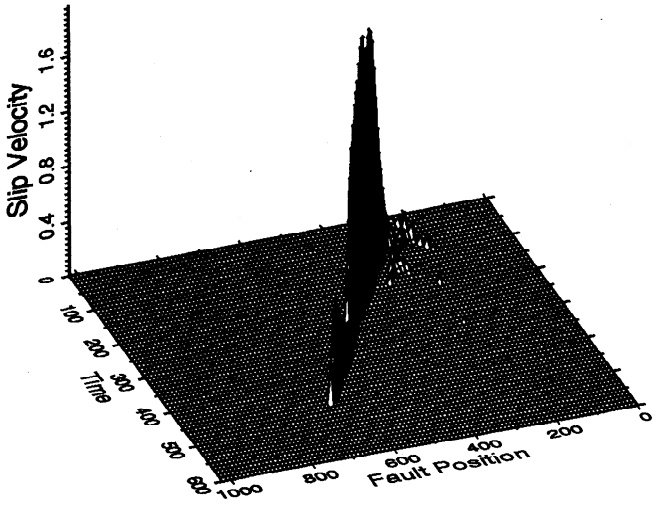

Figure 10. Another example of the slip velocity field for $\hat{T}_{sp} = 0.9$. It is in the form of a single self-healing *Heaton*'s [1990] pulse. Both ends of the rupture are far from the barriers.

any of the boundaries but are, instead, stopped very close to one of the boundaries by the stress depletion created there by the overshoot of a previous event having reached this boundary. An example of such a stress depletion can be seen in Figure 9 near position 1000.

For $\hat{T}_{sp}$ equal to or greater than 0.5, ruptures no longer occur in the form of crack-like ruptures. The rate dependence of the friction law becomes now strong enough to induce an abrupt locking of the fault very soon after the passage of the rupture front, i.e., before the arriving of the stopping phases. This mechanism was proposed by *Heaton* [1990] and was analyzed for

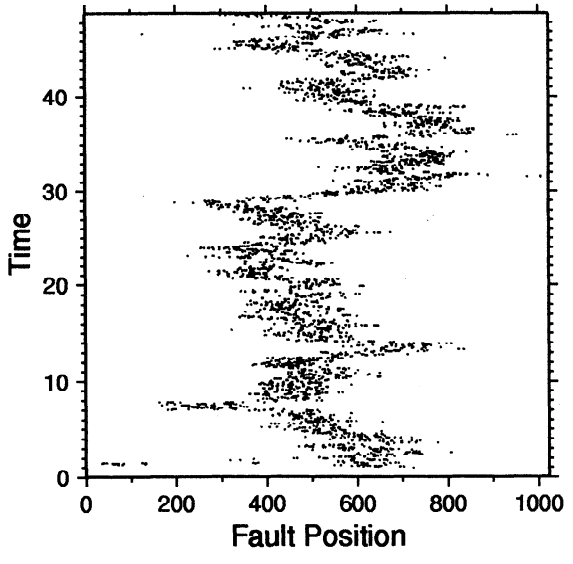

Figure 11. Time sequence of position of epicenters for $\hat{T}_{sp} = 0.9$. Each dot indicates the locus of one earthquake of the sequence. The epicenters are rarely located near the boundaries, and their positions are (weakly) correlated from event to event (see text).

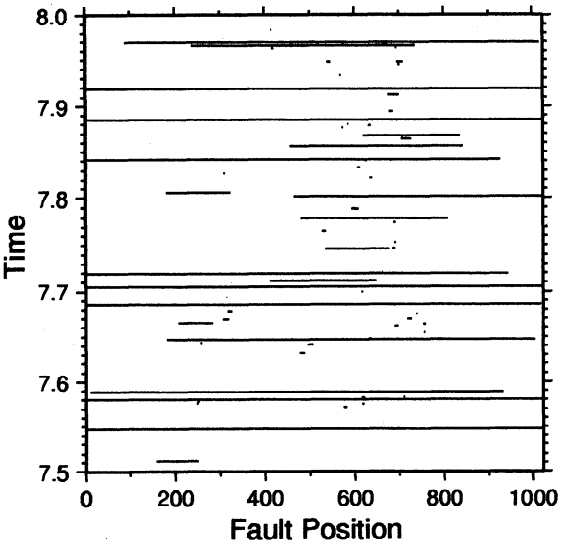

Figure 12. Seismicity on the fault as a function of time for a strong rate dependence of the constitutive law ($\hat{T}_{sp} = 0.9$). There are still a lot of events that break the whole fault, but there are some that break only part of it and which are not artifacts of the triggering procedure. Furthermore, the time sequence is also completely irregular.

antiplane faults by *Cochard and Madariaga* [1994]. It produces the typical narrow rupture episodes known as Heaton's pulses as shown in Figure 10 for $\hat{T}_{sp} = 0.9$. Because of this premature healing, the rehealed points receive waves from those still moving, just like the areas of the fault that have not ruptured yet. As a consequence, stress increases in the parts of the fault that have already healed and other pulses may be triggered in their trail, producing complex rupture sequences (see a two pulse rupture in Figure 13, for $\hat{T}_{sp} = 0.9$). Often, more than two pulses are observed. Often, also, bilateral propagation is observed. Another consequence of this stress increase due to premature healing is that after the event the stress remains higher near the epicenter, so that the next event is likely to be initiated again in the same region as the present one. It is thus observed, as in Figure 11 for $\hat{T}_{sp} = 0.9$, a slow migration of the epicenters. This peculiar behavior is very likely to disappear if we would introduce material heterogeneities (in the threshold, for instance) because the stress distribution near the end of an event depends, to first order, on the value of $\hat{T}_{sp}$ at this point, whereas, of course, the initiation is related to how far the final stress at one point is from the threshold.

From $\hat{T}_{sp} = 0.5$ to $\hat{T}_{sp} = 0.8$ the complexity gradually increases without any clear qualitative change. For $\hat{T}_{sp} = 0.5$ or 0.6 all of the (big) earthquakes of the cycles are stopped by at least one of the two edges of the fault or by the stress heterogeneity induced by it (see above). For $\hat{T}_{sp} = 0.7$ or 0.8, only one earthquake is stopped by none of the boundaries but, instead, only by the initial stress heterogeneities.

This is, however, the general situation with $\hat{T}_{sp} = 0.9$, as can be seen partly on the seismicity plot (Figure 12) for most of the events whose length is less than around 0.5, and this still happens frequently for greater lengths (of course, the greater the length, the more likely one of the boundaries is to play a part). The velocity and stress fields for one event of the cycle are shown in Figures 13 and 14, respectively. The slip velocity field of an event stopped far from the boundaries is shown in Figure 10. We can see how heterogeneous the stress field is at the end of the rupture. The persistence of stress heterogeneity after each successive event is clearly observed in Figure 15, which shows the final stress after each event in the time range displayed.

For greater clarity we now show, in figure Figure 16, slip velocity and stress as a function of time at point 400 of the fault during events shown on previous figures for $\hat{T}_{sp} = 0$ and $\hat{T}_{sp} = 0.9$. We clearly see overshoot when $\hat{T}_{sp} = 0$ and partial stress drop when $\hat{T}_{sp} = 0.9$.

Let us assume that $\mu = 3 \times 10^{10}$ Pa (300 bars), $\beta = 3 \times 10^3$ m/s, and $T_{thres} = 30$ MPa (300 bars). For $\hat{T}_{sp} = 0.9$ we have a maximum velocity (in Figure 16) $\hat{V} = 1.2$. Thus the "real" velocity is $(2T_{thres}/\mu)/\beta = 7.2$ m/s. If we further assume that the whole fault is 200 km long, then the risetime $\hat{t}_r$ at that particular point is $\Delta x/\beta \times \hat{t}_r \approx 1$ s (taking $\hat{t}_r = 193 - 178$). The dynamic stress drop at that point is about 90% of the total possible stress drop, i.e., about 27 MPa (270 bars). The static stress drop is only about 30% of the total stress drop, thus about 10 MPa (100 bars); but the average static stress drop is even less (see Figure 18) at about 0.1 (i.e., 10% of the total stress drop), hence 1 MPa (10 bars).

Properties of Complex Seismicity

We now discuss some statistical properties of the "complex" case of our model: $\hat{T}_{sp} = 0.9$. In Figures 17, 18, and 19 are plotted the seismic moment $\hat{M}$, the average stress drop $\Delta\hat{T}_{av}$ as a function of the broken patch $\hat{\ell}$, and the frequency-"magnitude" distribution, respectively. Figure 19 also shows the distribution with a smaller fault ($I = 513$), the friction parameters being the same.

With the value of $\Delta\hat{\sigma}$ used (0.05), the big events are not distinct from the "artificial" small events. However, we can guess from Figure 17 that the transition is at about $\hat{\ell} = 0.02$ (about 20 Δx), which corresponds to $\hat{M} = 0.005$, and as $\log_{10}(0.005) = -2.3$, we see

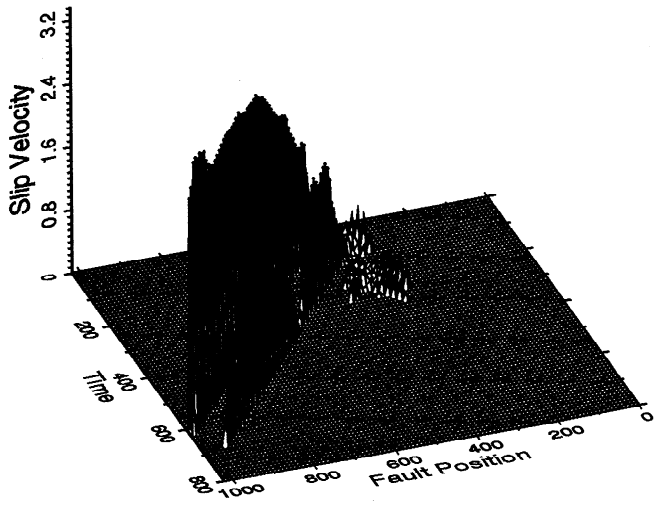

Figure 13. Slip velocity field for one event of the simulation for $\hat{T}_{sp} = 0.9$. It is in the form of two self-healing *Heaton*'s [1990] pulses.

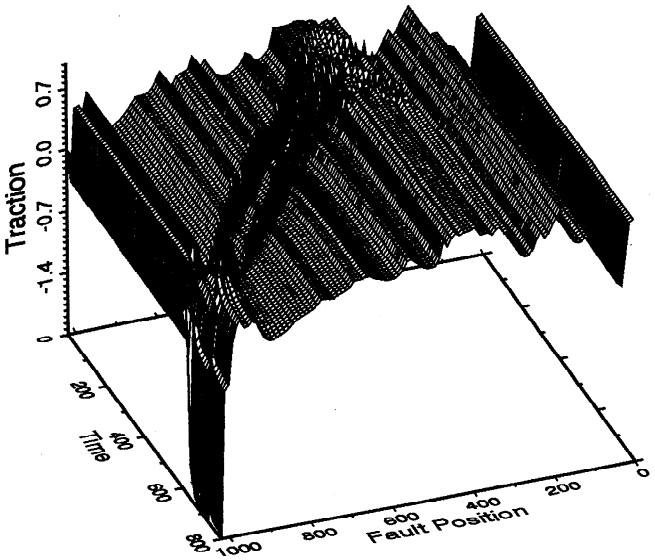

Figure 14. Stress field for the same event as in Figure 13 ($\hat{T}_{sp} = 0.9$). The stress is now heterogeneous enough on the fault plane in this case to stop the rupture at one end far from the geometrical barrier.

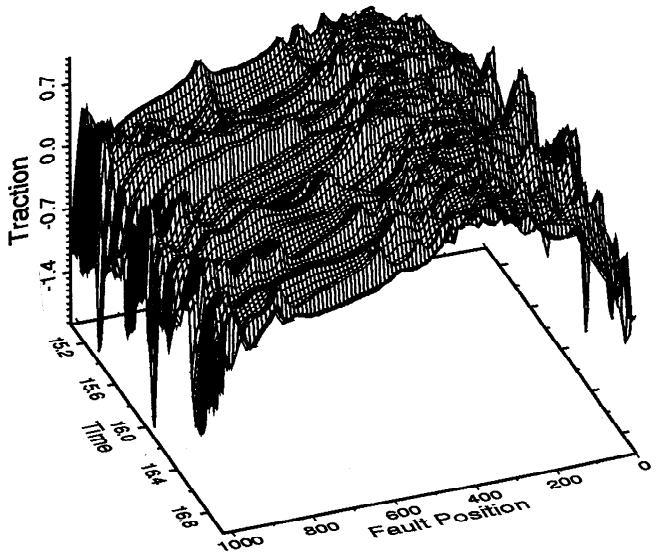

Figure 15. Stress field after each event in the time window shown for $\hat{T}_{sp} = 0.9$. We see how variable in space and time the stress field organizes itself. The lines are equally spaced in time owing to the plotting algorithm (to allow for better legibility).

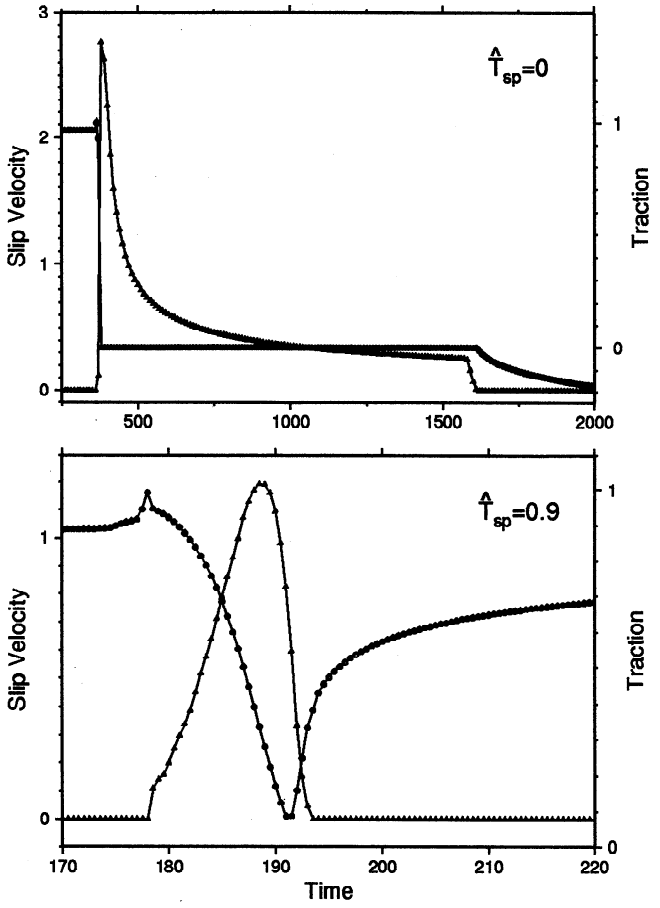

Figure 16. Slip velocity (triangles) and traction (circles) at point 400 of the fault (top) for $\hat{T}_{sp} = 0$ (corresponds to event shown in Figures 5 and 6) and (bottom) for $\hat{T}_{sp} = 0.9$ (corresponds to event shown in Figure 10). We see overshoot in the first case and partial stress drop in the second.

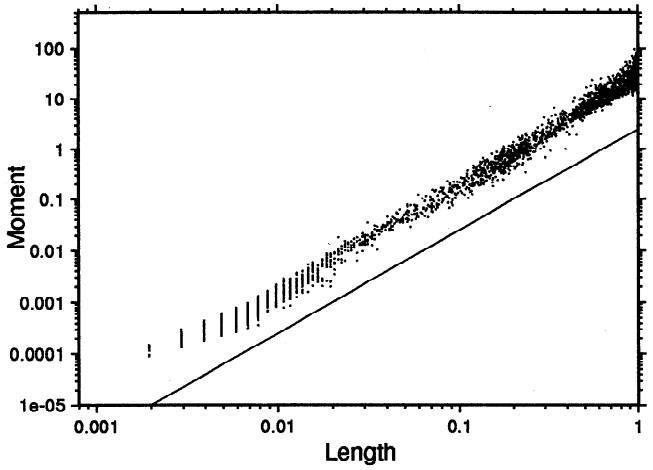

Figure 17. Moment length distribution for $\hat{T}_{sp} = 0.9$ and $\Delta\sigma = 5 \times 10^{-2}$. The straight line has a slope 2, thus showing that the distribution has the property extrapolated from nature to the present two-dimensional model.

$$\Delta T_{av} = \text{const} \times \mu \frac{\bar{D}}{\Lambda} \tag{17}$$

where Λ is a characteristic length of the rupture which can only be ℓ in our model, $\bar{D}$ is the average slip displacement, and the constant is of order 1. The seismic moment is

$$M = \mu \bar{D} \ell \,, \tag{18}$$

so having the moment M proportional to ℓ^2 is exactly equivalent to have ΔT_{av} constant. This is shown in Figure 18, where we plot stress drop as a function of patch

that it roughly corresponds also to the clear change in the frequency-magnitude relation at $\log_{10}(\hat{M}) = -2$. So, above this transition the seismic moment of these events is proportional to ℓ^2, which is expected for our 2-D model.

The frequency-magnitude plot (Figure 19) does not exhibit a Gutenberg-Richter behavior. Note, however, that just before the "bump" of big events at the right of Figure 19, there is a decrease of frequency with increasing magnitude. This happens in the range $-0.25 < \log_{10}(\hat{M}) < 0.5$, and the relation is roughly linear with a negative slope. The upper limit corresponds to $\hat{\ell} = 0.4$ (about 400 Δx), above which it is precisely observed that the effect of the boundaries becomes predominant. With the smaller fault the "depression" in the distribution is hardly visible at $\log_{10}(\hat{M}) = 0.5$. We can thus anticipate that this power law behavior would continue if we could increase the number of elements used in the simulations (still expecting a larger proportion of big events).

The static stress drop obeys the relation

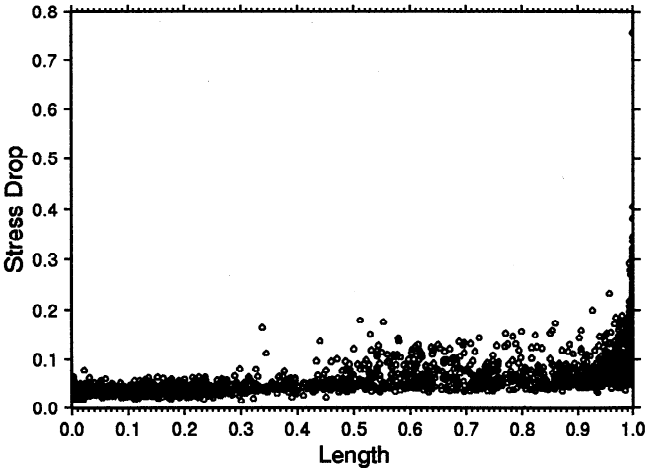

Figure 18. Stress drop length distribution for $\hat{T}_{sp} = 0.9$ and $\Delta\sigma = 5 \times 10^{-2}$. The stress drop is rather constant, as expected. The scatter for the events is due to the overshoot created by interaction with the boundaries. This overshoot is also responsible for the slightly smaller stress drop for events of length less than about 0.3. See text for details. (The point with $\hat{\ell} = 1$ and $\Delta\hat{T}_{av} > 0.7$ corresponds to the first event in the simulation.)

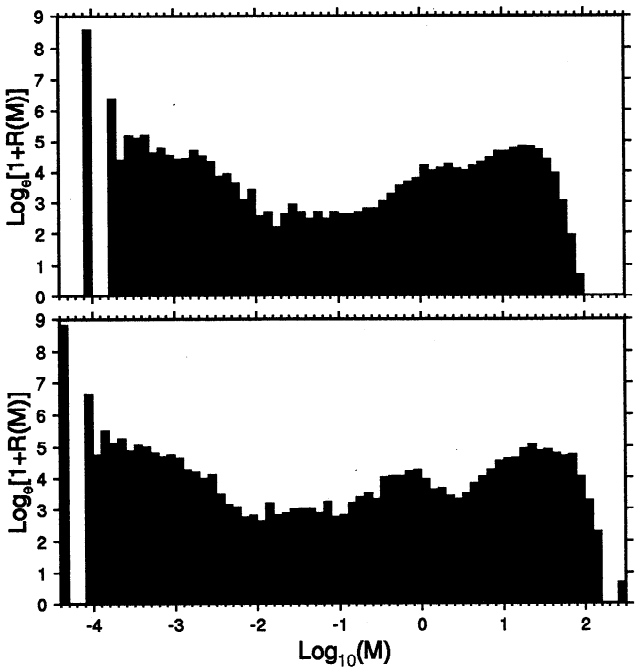

Figure 19. Frequency-magnitude distribution for $\hat{T}_{sp} = 0.9$, $\Delta\sigma = 5 \times 10^{-2}$, and two different discretizations (thus modeling two different fault sizes) using (top) 513 points and (bottom) 1025 points. The transition between small and big events is at about $\log_{10}(\hat{M}) = -2$. An interesting feature is the transition occurring at about $\log_{10}(\hat{M}) = 0.5$. It is scarcely visible for the small fault, but it is seen much better for the large one.

length ℓ. The scatter for the big events is due to the interaction with the edges of the fault: when a pulse reaches one of the edges, the overshoot gives rise to a very important stress drop (see Figure 14) compared to the case when it is stopped more gradually by stress heterogeneities. The even greater scatter at the right of the distribution is because events of length equal to the total length obviously reach the two boundaries. Nevertheless, the overshoot is still larger when the rupture is being stopped by a strong stress depletion like the one near the barriers than when the depletion is milder, which is the situation near the center of the fault. (A strong barrier is equivalent to an infinitely deep stress depletion.) This is the reason why stress drop is a little lower for events with length less that about 0.3. The probability for an event exceeding this limit to interact with one of the boundaries increases, of course, with length.

Considering again relation (18) for the moment, the relation $M \propto \ell^2$ is also equivalent to have $\bar{D} \propto \ell$. This would be the expected result with a crack-like rupture propagation, and it is indeed the argument used to explain the scaling law $M \propto \ell^3$ in the (3-D) real Earth for earthquakes with $\ell < W$, W being the width of the seismogenic crust. When the propagation is crack-like, the risetime is controlled by stopping phases coming from the edge of the rupture; so the larger the rupture, the longer the risetime, and, consequently, the bigger $\bar{D}$. It is much more surprising that $\bar{D} \propto \ell$ when the propagation is in the form of short risetime self-healing pulses. The rupture propagation, in fact, "adjusts" itself to satisfy the scaling law. This can be done with a varying risetime, a varying slip velocity, or even by a rupture with two or more pulses in sequence (which is, in fact, another way of varying the risetime). This is an argument to suggest that we have reached a state resembling that of self-organized criticality even if the dynamic range reached is still too small to allow for definitive conclusions. In the earth, for earthquakes with $\ell > W$, it is not clear yet if the scaling law satisfies $M \propto W\ell^2$ as suggested by *Scholz* [1982, 1994] and *Pegler and Das* [1996] or $M \propto W^2\ell$ as suggested by *Romanowicz* [1992]. The former relation implies $\bar{D} \propto \ell$, while the later implies $\bar{D} \propto W = \text{const}$. So our results are certainly consistent with the scaling $M \propto W\ell^2$ and also provide a natural physical explanation to this surprising scaling as suggested by *Heaton* [1990].

Let us also remark that for the Burridge-Knopoff model (1-D spring-block chain but to be compared in this respect with our 2-D model) the scaling relation tends to be $M \propto \ell$ for the large events (*Carlson et al.* [1991, Figure 9], velocity-weakening friction used). This is most probably due to the flat springs (strength k_p) linking each block to the driving block, which introduce another length scale in the problem (T_{thres}/k_p). For the big events the displacement of the blocks become high enough for these spring to prevent them from going farther and so the displacement D tends to be independent of the length of the event. The same happens in a more sophisticated version of the Burridge-Knopoff model including long-range interactions (*Langer et al.* [1996], slip-weakening friction used). In fact, these flat springs can be seen as an approximate modeling of the coupling of the crust to the underlying substrate [*Lehner et al.*, 1981; *Johnson*, 1992], and their effects are similar to what happens when the friction is not or is not enough rate-dependent [*Rice and Ben-Zion*, 1996]: the propagation is in the form of an enlarging crack, so that the stress concentration at the crack tip scales with the ruptured area and makes the rupture unstoppable until it reaches the edge of the fault; then interaction with the boundaries (the analog to the coupling due to the flat spring) may (or may not) allow for the stress fluctuations to stop the rupture. Notice that after reaching the boundaries the rupture is in the form of a (very large) pulse [*Day*, 1982]. In our case the friction has enough rate dependence to induce healing very soon and thus allows for narrow propagating pulses. Thus the stress concentration scales only with the (rather constant) "width" of the pulse and is thus much lower than for an enlarging crack. This explains why the propagation is more easily stopped by (potentially weaker) stress heterogeneities.

For rate-independent friction ($\hat{T}_{sp} = 0$), static and

dynamic stress drop are almost the same. Actually, for antiplane faults, static stress drop overshoots the dynamic stress drop by about 24%. For higher values of $\hat{T}_{sp}$ the fault locks prematurely, so that static stress drop becomes less that the dynamic one and varies significantly from point to point. This lateral variation develops because slip arrest occurs locally, not in response to stopping phases propagating inside the fault that introduce a correlation between neighboring points. Because of this early, disorganized healing, the final slip at neighboring points on the fault may be quite variable. Since, roughly speaking, stress changes on the fault are related to the gradient of slip, even small variations of slip can produce strong heterogeneities in the static stress field after the event. Since stress can only change inside a limited range ($0 < T < T_{thres}$), these lateral variations put some fault elements closer to rupture than others. As a consequence, the future seismicity of the fault is completely determined by these heterogeneities in the residual stress field. Thus the mechanism that generates complexity in our model is clearly identified. We propose that the key to the creation of heterogeneity in our model is partial stress drop. This is not at all a new concept in seismology: *Brune* [1970] proposed from observational arguments that most earthquakes presented partial stress drop and suggested that dynamic stress drop (the maximum is T_{thres} in our case) was much larger than static stress drop, and this seems to have been confirmed by more recent studies [*Ramón Zúñiga*, 1993]. The main difference between our results and the suggestion by *Brune* [1970] is that he considered a model where partial stress drop was uniform along the fault, while in our models, partial stress drop triggers strong lateral variations of static stress drop.

Note that the fault is assumed to be clamped at the ends by unbreakable barriers, and we cannot exclude the possibility that this plays a significant part in the behavior of the model. Even if this were the case, such a configuration would be intended to model a deeply buried fault as, e.g., in a subduction zone, whereas a fault with one free boundary would more likely model a fault such as the San Andreas fault as in the work by *Rice and Ben-Zion* [1996]. (A complete modeling should, of course, include a transition from an elastic material to a plastic one to avoid infinitely increasing stresses out of the fault (in the barriers).)

Summary

We have demonstrated that for certain highly rate-dependent friction laws a simple antiplane fault embedded in a homogeneous medium can spontaneously become complex. This complexity has several interesting features:

1. Premature locking of the fault occurs, so that slip duration at any point of the fault is independent of the total size of the fault. Premature healing is associated with partial stress drop, so that stress heterogeneity may be simply due to the extreme sensitivity of fault stress to very small changes in the slip distribution. Premature healing is also associated with the generation of self-healing pulses proposed by *Heaton* [1990] and explained in our previous work [*Cochard and Madariaga*, 1994].

2. Stress heterogeneity and partial stress drop are manifestations of the same underlying instability. Partial stress drop occurs for all friction models that have a strong rate-dependent friction. Partial stress drop disorganizes the fault for the simple reason that stress drop of neighboring points will be highly variable.

3. Slip gradient (dislocation density) and stress heterogeneity appear when small-scale modes of slip on the fault can express themselves. For full stress drop models like rate-independent friction laws, these small-scale modes are suppressed by the requirement that stress drop be fixed and uniform and determined only by the constitutive parameters. In that case, only material heterogeneity can produce complexity.

4. Seismic events, i.e., events whose length is greater than the length of the "nucleation" zone follow an ℓ^2 scaling law, in which seismic moment scales like the product of partial stress drop and the square of the length of the zone that actually slipped during the event. Thus the regularization length that is included in our slip-weakening model has no influence on the properties of large seismic events. The rupture propagation of these events "adapts" its slip velocity or risetime to satisfy the scaling law.

In conclusion, we have shown that a rate-dependent friction can spontaneously produce heterogeneity for large values of a control parameter. At the other extreme, the rate-independent friction suppresses these instabilities for the very simple reason that partial stress drop is eliminated from the outset. It is very likely that both material heterogeneities and dynamically generated complexity play a role in determining the observed complexity of faulting and seismic events. Given the sparse knowledge that we currently have about the friction laws at high slip rates in real faults, we firmly believe that heterogeneity should be explored without preconceived assumptions about which material and dynamically generated heterogeneity dominates in the Earth. We anticipate that complexity will develop much more easily in three dimensions and (based on a few preliminary studies) that in the presence of a small degree of material heterogeneities, a smaller degree of rate dependence would be necessary to generate complexity that would not exist without this rate dependence.

Appendix: Does the Instantaneous Initial Stress Drop Have Any Influence?

As already mentioned above, the small stress drop ($\Delta\sigma$) at the initiation of slip was introduced to reduce computer time and storage. We show here that this

procedure changes only the properties of the small-event distribution but does not affect the properties of large events.

If $\Delta\sigma$ were 0, then an element of the fault reaching the friction threshold would not move dynamically immediately; instead, it would slowly accelerate, driven quasi-statically by the increase of $T_{\text{ext}}(x,t)$. As this element slips, it drives its neighbors, in turn, to the threshold, creating a larger and larger zone of creeping elements. As the size of the slipping patch increases, it will eventually reach the so-called nucleation length. This is the minimum patch that can become unstable and break dynamically. For antiplane faults and pure slip weakening this patch length is approximately given by $(2\mu U_0)/(\pi T_{\text{thres}})$ [e.g., *Dieterich*, 1992], around 13 in our nondimensional units. Since the numerical solution of the integral equation (8) is controlled by the faster timescales present in it, the slow evolution of the fault in the interseismic period would have to be computed at the time step (constant in our simulation) that is appropriate for the dynamic regime and is several orders of magnitude less than those that are actually needed. Equations of this type are called stiff and require special techniques for their solution as shown by *Tse and Rice* [1986] for a spring loaded massive slider.

When $\Delta\sigma \neq 0$, dynamic events that involve a single fault element become possible, since no length scale acts during the small initial stress drop. We thus see in Figure 3 events of all sizes, ranging from one element to the total size of the fault. What happens if we decrease the magnitude of $\Delta\sigma$? The moment/size distribution is shown in Figure A1 for $\hat{T}_{\text{sp}} = 0.95$ with three values of $\Delta\hat{\sigma}$ (5×10^{-2}, 5×10^{-3}, and 5×10^{-4}). For clarity of the figure the plots have been shifted in the vertical direction. The diamonds near the end of each distribution have the same coordinates and indicate a slope 2 in this bilogarithmic plot. For $\Delta\hat{\sigma} = 5\times10^{-2}$ the whole distribution thus approximately obeys the same statistics. For $\Delta\hat{\sigma} = 5\times10^{-3}$ we can discern a cluster of small events of size $\hat{\ell}$ less than 0.03. For $\Delta\hat{\sigma} = 5\times10^{-4}$ the cluster of small events, of size less than 0.05, is clearly distinct from the larger events. The form of the distribution for the small events changes, and its width slowly increases with diminishing $\Delta\sigma$. On the other hand, the distribution of large events remains unaffected by the variation of $\Delta\sigma$. In our previous paper [*Madariaga and Cochard*, 1996], $\Delta\sigma$ was different from zero only for the first point initiating an event. The large-event distribution of Madariaga and Cochard showed the same properties as here, an additional proof that the small triggering stress drop does not affect the large-event dynamics.

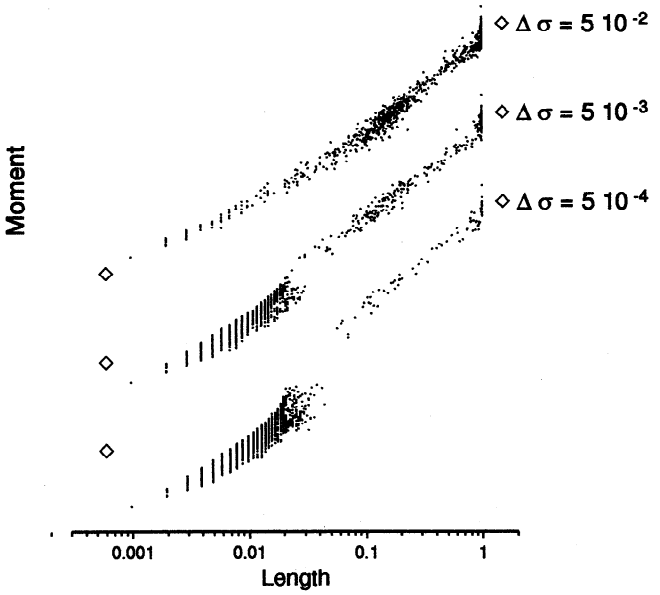

Figure A1. Influence of the small initial stress drop $\Delta\sigma$ for $\hat{T}_{\text{sp}} = 0.95$. The seismic moment is shown as a function of rupture length for three different values of $\Delta\sigma$. For clarity the plots have been shifted in the vertical direction. The diamonds near the end of each distribution have the same coordinates, and the straight line joining those of each distribution has a slope 2. Diminishing $\Delta\sigma$ leads to an increase of the proportion and a change in the statistical properties of the small (artificial) events but does not alter the statistics for the big events.

The main consequence of the introduction of the small artificial stress drop $\Delta\sigma$ at the beginning of rupture is to produce a large number of small events. The number of these small events increases as $\Delta\sigma$ decreases. This zone, also present in the Burridge-Knopoff model and whose length is sometimes referred to by "delocalization" or "correlation" length [*Carlson and Langer*, 1989; *Carlson et al.*, 1991], is the analog of the nucleation zone. If we could solve the integral equation with $\Delta\sigma = 0$, all the small events preceding a big one would collapse into a single, slowly creeping initiation phase.

Beside the fact that the friction law used is not pure slip weakening, the difference between the theoretical (quasi-static approximation) value for the nucleation size and the one actually observed is due to $\Delta\sigma$. After each small event, the next one will, of course, be started from a locked fault, i.e., with zero kinetic energy, and the process of building the "nucleation zone" has to be started again from the beginning. The kinetic energy from the previous small events is lost, so more potential energy has to be stored; the nucleation zone takes longer to be built and is larger. If, on the contrary, $\Delta\sigma$ is big enough and/or the stress field at the time of initiation of an event is homogeneous enough, a big event can be triggered directly, i.e., without any small event before it. This is what has happened for $\hat{T}_{\text{sp}} = 0$ and 0.1 and $\Delta\hat{\sigma} = 0.05$ (see section on seismicity with increasing rate dependence). This point has another independent, interesting consequence: that the nucleation zone takes longer to be built means that the ambient stress field will be higher when the big event is eventually triggered. So this big event will be able to propagate further (everything else being equal), and so

complexity will not be favored compared with the case $\Delta\sigma = 0$.

It has been proposed by *Perrin et al.* [1995] to modify the BIE (1) in order to separate the quasi-static term from the dynamic one so that it is possible to incorporate the dynamic solution (highly computer time and memory consuming) only when its contribution becomes nonnegligible. This has been implemented and used by *Rice and Ben-Zion* [1996], so that it is now possible to render $\Delta\sigma$ exactly zero.

The foregoing discussion makes us confident that the statistical properties of the large events in our model are not affected by $\Delta\sigma$. In all the other computations presented in this paper we used $\Delta\hat{\sigma} = 5 \times 10^{-2}$, which is big enough to allow for large catalogs of events.

Notations

β shear wave speed.
Γ ruptured domain at a given time.
ϵ tectonic stress rate.
ϵ_t time collocation parameter, $\in [0, 1]$.
$\theta(x,t)$, θ_0 state variable (dimension of velocity), value of it such that if $\theta < \theta_0$, velocity weakening begins (if $D > U_0$).
μ rigidity of the medium.
ρ density of the medium.
$\sigma(x,t)$ stress tensor.
$\Delta\sigma$ instantaneous stress drop at the beginning of slip.
τ dummy time variable.
ξ dummy in plane parallel to displacement spatial coordinate.
$D(x,t)$ displacement discontinuity, $= u_y(x, z = 0^+, t) - u_y(x, z = 0^-, t)$.
$\bar{D}$ average (over the broken patch) of slip for an event.
D_c length scale in the friction law, related to the velocity-weakening process.
h dimensionless time step, $= \beta\Delta x/\Delta t$.
i, j discrete space variables along the x axis.
I total number of points used to discretize the fault (=1025 most of the time).
$K(x,t)$ space-time convolution kernel.
ℓ broken patch length for an event.
L total length of the fault.
m, n discrete time variables.
M seismic moment for an event.
$S(x,t)$ space-time convolution.
t, Δt time variable, time step.
$T_{\mathrm{abs}}(x,t)$ absolute stress.
$T_{\mathrm{ext}}(x,t)$ external (loading) stress.
$\Delta T(x,t)$ difference between the two above.
ΔT_{av} average (over the broken patch) stress drop for an event.
T_{sp} stress parameter indicating the magnitude of the velocity weakening.
$u = u_y$ component of displacement along y.
U_0 slip-weakening parameter.
$V(x,t)$ rate of displacement discontinuity, $= \dot{D}(x,t)$.
x, y, z in plane perpendicular and parallel to displacement and out of plane spatial coordinates.
Δx grid spacing.

Acknowledgments. We benefited from discussions with Jean-Pierre Vilotte, Yehuda Ben-Zion, Jim Rice, Bruce Shaw, and Gutuan Zheng and from e-mails involving mainly J. Rice and Jim Langer and, also, Y. Ben-Zion, Leon Knopoff, Chris Myers, and B. Shaw. We also thank Tom Heaton, Greg Beroza, and Steven Roecker who reviewed the manuscript and helped to improve the presentation. This research was sponsored by contract SCI from the EEC and computer time contributed by the Centre National de Calcul Parallèle en Sciences de la Terre. This paper was completed while A. C. was a postdoctoral fellow at Harvard University with grants from the French Ministère de l'enseignement supérieur et de la recherche and from grants N00014-90J-1379 and 1434-94-G-2450 from the Office of Naval Research and U.S. Geological Survey, respectively.

References

Andrews, D. J., Rupture velocity of plane strain shear cracks, *J. Geophys. Res.*, *81*, 5679–5687, 1976.

Andrews, D. J., Dynamic plane-strain shear rupture with a slip-weakening friction law calculated by a boundary integral method, *Bull. Seismol. Soc. Am.*, *75*, 1–21, 1985.

Andrews, D. J., and Y. Ben-Zion, Wrinkle-like slip pulse on a fault between different materials, *J. Geophys. Res.*, in press 1996.

Beeler, N. M., and T. E. Tullis, Self-healing slip pulses in dynamic rupture models due to velocity-dependent strength, *Bull. Seismol. Soc. Am.*, pp. 1130–1148, 1996.

Ben-Zion, Y., and J. R. Rice, Earthquake failure sequences along a cellular fault zone in a three-dimensional elastic solid containing asperity and nonasperity regions, *J. Geophys. Res.*, *98*, 14,109–14,131, 1993.

Brune, J. N., Tectonic stress and the spectra of seismic shear waves from earthquakes, *J. Geophys. Res.*, *75*, 4997–5009, 1970.

Burridge, R., and L. Knopoff, Model and theoretical seismicity, *Bull. Seismol. Soc. Am.*, *57*, 341–371, 1967.

Carlson, J. M., and J. S. Langer, Mechanical model of an earthquake fault, *Phys. Rev. A*, *40*, 6470–6484, 1989.

Carlson, J. M., J. S. Langer, B. E. Shaw, and C. Tang, Intrinsic properties of a burridge-knopoff model of an earthquake fault, *Phys. Rev. A*, *44*, 884–897, 1991.

Cochard, A., and R. Madariaga, Dynamic faulting under rate-dependent friction, *Pure Appl. Geophys.*, *142*, 419–445, 1994.

Das, S., and K. Aki, Fault plane with barriers: A versatile earthquake model, *J. Geophys. Res.*, *82*, 5658–5670, 1977.

Das, S., and B. K. Kostrov, An investigation of the complexity of the earthquake source time function using dynamic faulting models, *J. Geophys. Res.*, *93*, 8035–8050, 1988.

Day, S. M., Three-dimensional finite difference simulation of fault dynamics: Rectangular faults with fixed rupture velocity, *Bull. Seismol. Soc. Am.*, *72*, 705–727, 1982.

Dieterich, J. H., Earthquake nucleation and faults with rate- and state-dependent strength, *Tectonophysics*, *211*, 115–134, 1992.

Heaton, T. H., Evidence for and implications of self-healing pulses of slip in earthquake rupture, *Phys. Earth Planet. Inter.*, *64*, 1–20, 1990.

Johnson, E., The influence of the lithospheric thickness on bilateral slip, *Geophys. J. Int.*, *108*, 151–160, 1992.

Kanamori, H., and G. S. Stewart, Seismological aspects of the Guatemala earthquake of February 4, 1976, *J. Geophys. Res.*, *83*, 3427–3434, 1978.

Langer, J. S., J. M. Carlson, C. R. Myers, and B. E. Shaw, Slip complexity in dynamic models of earthquake faults, *Proc. Natl. Acad. Sci. U.S.A.*, *93*, 3825–3829, 1996.

Lehner, F. K., V. C. Li, and J. R. Rice, Stress diffusion along rupturing plate boundaries, *J. Geophys. Res.*, *86*, 6155–6169, 1981.

Madariaga, R., Dynamics of an expanding circular fault, *Bull. Seismol. Soc. Am.*, *66*, 639–666, 1976.

Madariaga, R., and A. Cochard, Dynamic friction and the origin or the complexity of earthquake sources, *Proc. Natl. Acad. Sci. U.S.A.*, *93*, 3819–3824, 1996.

Melosh, H. J., Acoustic fluidization: A new geological process, *J. Geophys. Res.*, *84*, 7513–7520, 1979.

Melosh, H. J., Dynamical weakening of faults by acoustic fluidization, *Nature*, *379*, 601–606, 1996.

Nielsen, S., L. Knopoff, and A. Tarantola, Model of earthquake recurrence: Role of elastic wave radiation, relaxation of friction and inhomogeneity, *J. Geophys. Res.*, *100*, 12,423–12,430, 1995.

Okubo, P. G., Dynamic rupture modeling with laboratory-derived constitutive relations, *J. Geophys. Res.*, *94*, 12,321–12,335, 1989.

Pegler, G., and S. Das, Analysis of the relationship between seismic moment and fault length for large crustal strike-slip earthquakes between 1977-1992, *Geophys. Res. Lett.*, *23*, 905–908, 1996.

Perrin, G., J. R. Rice, and G. Zheng, Self-healing slip pulse on a frictional surface, *J. Mech. Phys. Solids*, *43*, 1461–1495, 1995.

Ramón Zúñiga, F., Frictional overshoot and partial stress drop. Which one?, *Bull. Seismol. Soc. Am.*, *83*, 939–944, 1993.

Rice, J. R., Spatio-temporal complexity of slip on a fault, *J. Geophys. Res.*, *98*, 9885–9907, 1993.

Rice, J. R., and Y. Ben-Zion, Slip complexity in earthquake fault models, *Proc. Natl. Acad. Sci. U.S.A.*, *93*, 3811–3818, 1996.

Romanowicz, B., Strike-slip earthquakes on quasi-vertical transcurrent faults: Inferences for general scaling relations, *Geophys. Res. Lett.*, *19*, 481–484, 1992.

Ruina, A., Slip instability and state variable friction laws, *J. Geophys. Res.*, *88*, 10,359–10,370, 1983.

Scholz, C. H., Scaling laws for large earthquakes: Consequences for physical models, *Bull. Seismol. Soc. Am.*, *72*, 1–14, 1982.

Scholz, C. H., A reappraisal of large earthquake scaling, *Bull. Seismol. Soc. Am.*, *84*, 215–218, 1994.

Shaw, B. E., Frictional weakening and slip complexity in earthquake faults, *J. Geophys. Res.*, *100*, 18,239–18,251, 1995.

Shibazaki, B., and M. Matsu'ura, Spontaneous processes for nucleation, dynamic propagation, and stop of earthquake rupture, *Geophys. Res. Lett.*, *19*, 1189–1192, 1992.

Tse, S. T., and J. R. Rice, Crustal earthquake instability in relation to the depth vatiation of frictional slip properties, *J. Geophys. Res.*, *91*, 9452–9472, 1986.

Vidale, J. E., W. L. Ellsworth, A. Cole, and C. Marone, Variations in rupture process with recurrence interval in a repeated small earthquake, *Nature*, *368*, 624–626, 1994.

Virieux, J., and R. Madariaga, Dynamic faulting studied by a finite difference method, *Bull. Seismol. Soc. Am.*, *72*, 345–369, 1982.

A. Cochard, Division of Applied Sciences, Harvard University, 29 Oxford Street, Cambridge, MA 02138. (e-mail cochard@esag.harvard.edu)

R. Madariaga, Département de Sismologie, Institut de Physique du Globe de Paris, 4, Place Jussieu, Case 89, 75252 Paris CEDEX 05, France. (e-mail madariag@ipgp.jussieu.fr)

(Received December 5, 1995; revised June 27, 1996; accepted July 2, 1996.)